PROCEEDINGS OF SCIENCE

OBSERVATION OF THE ^{26}Al EMISSION DISTRIBUTION THROUGHOUT THE GALAXY WITH INTEGRAL/SPI

Laurent Bouchet*, **Elisabeth Jourdain, Jean-Pierre Roques**
Université de Toulouse, UPS-OMP, IRAP, Toulouse, France
CNRS, IRAP, 9 Av. colonel Roche, BP 44346, F-31028 Toulouse cedex 4, France
E-mail: lbouchet@irap.omp.eu

We present the ^{26}Al map distribution throughout the Galaxy measured by the SPI spectrometer aboard the *INTEGRAL* observatory. This emission at 1.809 MeV is associated with the ^{26}Al decay and the production of heavy elements in the Galaxy. The only available ^{26}Al map to date has been released, more than fifteen years ago, thanks to the *COMPTEL* instrument. However, at the present time, SPI offers a unique opportunity to enrich this first result. The data accumulated between 2003 and 2013 which amounts to 2×10^8s of observing time are used to perform a dedicated analysis, aiming to deeply investigate the spatial morphology of the ^{26}Al emission. The data are first compared with several sky maps based on observations at various wavelengths.
For most of the distribution models, the inner Galaxy flux is compatible with a value of 3.3×10^{-4} ph cm^{-2} s^{-1} while the preferred template maps correspond to young stellar components such as core-collapse supernovae, Wolf-Rayet and massive AGB stars. To get more details about this emission, an image reconstruction is performed using an algorithm based on the maximum-entropy method. In addition to the inner Galaxy emission, several excesses suggest that some sites of emission are linked to the spiral arms structure. Lastly, an estimation of the ^{60}Fe line flux, assuming a spatial distribution similar to ^{26}Al line emission, results in a ^{60}Fe to ^{26}Al ratio around 0.14, which agrees with the most recent studies and with the SN explosion model predictions.

The 34th International Cosmic Ray Conference,
30 July- 6 August, 2015
The Hague, The Netherlands

*Speaker.

PoS(ICRC2015)896

1. INTRODUCTION

To date, only the *COMPTEL* Compton telescope aboard the Compton Gamma Ray Observatory has mapped the ^{26}Al during its nine years survey. The emission has been found mainly distributed along the Galactic plane and supports a massive-stars origin ([1, 2, 3, 4]). In addition, the early *COMPTEL* sky maps suggest many spots, some of them being potentially associated with the Galactic spiral arms structure [5]. However, while the main features of the *COMPTEL* map are set with confidence, the low-intensity features need to be confirmed.
In this paper, 10 years of *INTEGRAL* observation are used to attempt to examine the spatial morphology of the ^{26}Al line, through direct sky-imaging and sky model comparison.

2. INSTRUMENT, OBSERVATIONS AND DATA ANALYSIS

The SPI spectrometer ([7, 8]) observes the sky in the 20 keV to 8 MeV range. In addition to its spectroscopic capabilities, the telescope can image the sky with a spatial resolution of $\sim 3^\circ$ (FWHM) over a field-of-view of 30° thanks to a coded-mask aperture. The analysis presented is based on the data accumulated between 2003 and 2013, which represent 2×10^8s of observations. This corresponds to 80 000 exposures of $\sim$45 minutes each.
The signal recorded by the SPI camera on the 19 Ge detectors is composed of contributions from each source (point-like or extended) present in the field of view, convolved by the instrument aperture, plus the background. To determine the sky model parameters, we adjust the data through a multi-component fitting algorithm, based on the maximum likelihood statistics. The instrumental background is the main contributor to the flux recorded by the detector plane and a key issue since the signal-to-noise ratios considered in this study are below 1%. A special attention is paid to the background intensity variation with time, thanks to the development of a specific algorithm which aims to minimize the number of parameters used to model it. The Ge detectors relative count-rate due to the instrumental background (hereafter the detector pattern) is stable on a time-scale of $\sim$6 months. This pattern is fixed by using empty-field like observation (fixed-pattern) or adjusted during the fitting process (fitted-pattern; more free parameters). We compared the results of both methods. The details on the analysis are described in [9].

3. COMPARISON OF THE ^{26}Al EMISSION WITH TEMPLATES

It consists of using template maps to model the spatial distribution of the ^{26}Al emission through the Galaxy. For the fixed-pattern method, this leads to a ^{26}Al detection significance of $\sim 23\sigma$ with a $\chi^2_L/dof = 1.004$. Each template leads to a significant detection, the worse template (H_I) has a significance of âĹij $\sim 17\sigma$. The same analysis for the fitted-pattern gives ^{26}Al detection significance of $\sim 18\sigma$ with a $\chi^2_L/dof = 0.997$ for the best templates. Figure 1 (Top) displays the Maximum Likelihood Ratio (MLR) obtained with both pattern determination methods (fixed and fitted-pattern) for each of the tested maps (ordered by increasing contrast). The chi-square curves follows the same evolution regardless the background determination method and hence that the conclusions do not depend much on it. Several maps lead to similar results and we could say that star related distributions (FIR and MIR maps, dust and free-free distributions, all with rather

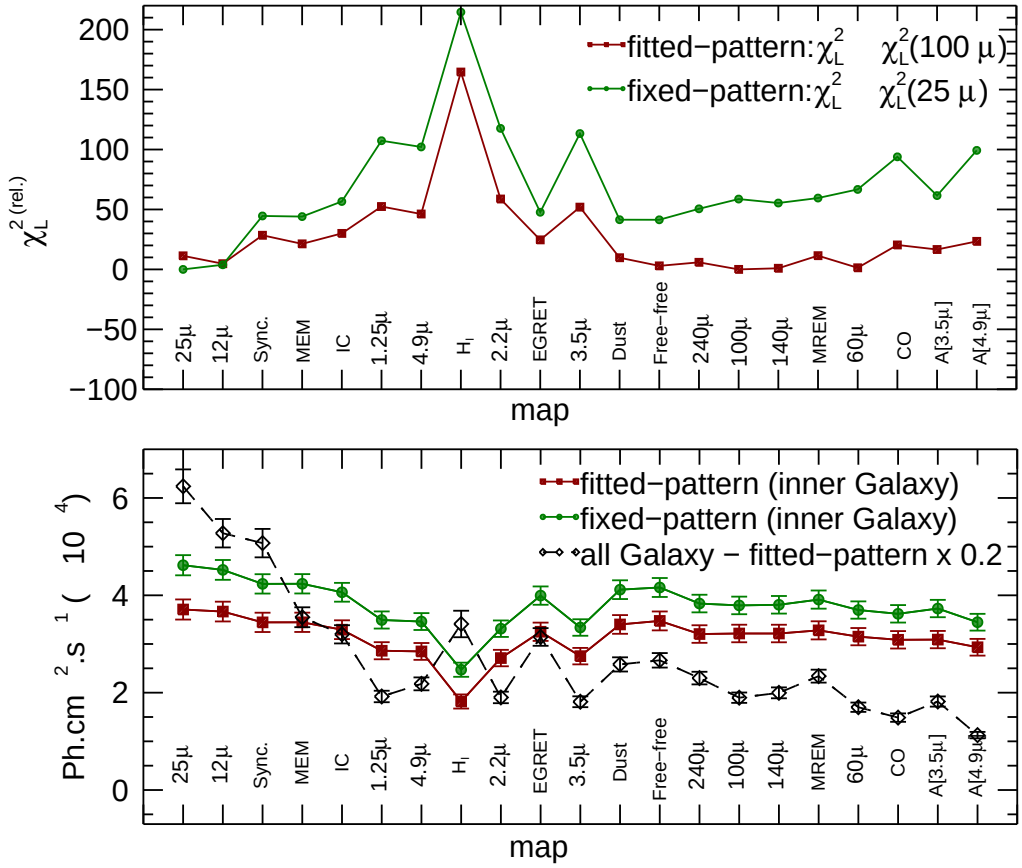

Figure 1: Figure 1: (Top) The relative chi-square variation ($\chi_L^{2(rel.)}$)) versus the assumed template used to model the distribution ^{26}Al line. $\chi_L^{2(rel.)}$) is the χ_L^2 from which the value of the best-fitted template is subtracted. The maps are ordered following their contrast defined as the ratio of the flux enclosed in the region $|l| \leq 150°$, $|b| \leq 15°$ to the total flux enclosed in $|l| \leq 180°$,$|b| \leq 90°$. Terms sync., dust and free-free, are abbreviations for 53 GHz synchrotron, dust and free-free maps. MEM and MREM indicate the *COMPTEL* maps, A[3.5μ] and A[4.9μ] symbols are for corrected NIR extinction maps (3.5 and 4.9μ). The red curve is for the fitted-pattern and green for fixed-pattern method. The best template is the 100μ template for the fitted-pattern method, and the 25μ template for the fixed-pattern method. (Bottom) Flux in the inner-Galaxy ($|l| \leq 30°$,$|b| \leq 10°$) in function of the map used to model the distribution of the ^{26}Al line. The dashed black-curve is the total flux in the Galaxy (fitted-pattern), scaled by a factor 0.2.

high-contrast) give a good description of the data, as expected from what we know about the ^{26}Al emission process. Similarly, 25μ and 12μ maps constitute good tracers, while presenting a low-contrast. In other hand, H_I and 53 GHz synchrotron maps can be excluded.

We note that distributions built by imaging method (MEM or MREM) from *COMPTEL* data remain good tracers of the ^{26}Al emission. As shown on Figure 1 (Bottom), the reconstructed flux attributed to the inner Galaxy does not depend much on the template map used and is compatible with a value of $3.3\times\ 10^{-4}$ph cm^{-2} s^{-1} , in agreement with the previously reported values. However, the total flux integrated over the whole sky clearly depends on the contrast of the assumed model. The more the map is contrasted (from left to right on Figure 1), the weaker is the reconstructed total flux.

This is due to the fact that the recovered global intensity relies on the central parts of the image (both higher flux and signal to noise ratios) and that a contrasted map encompasses less flux in its external parts than a flatter map.

4. SKY IMAGING

We performed a direct imaging reconstruction of the ^{26}Al emission by using a maximum-entropy method. The code is based on [10] algorithm and is described in [9]. The image presented

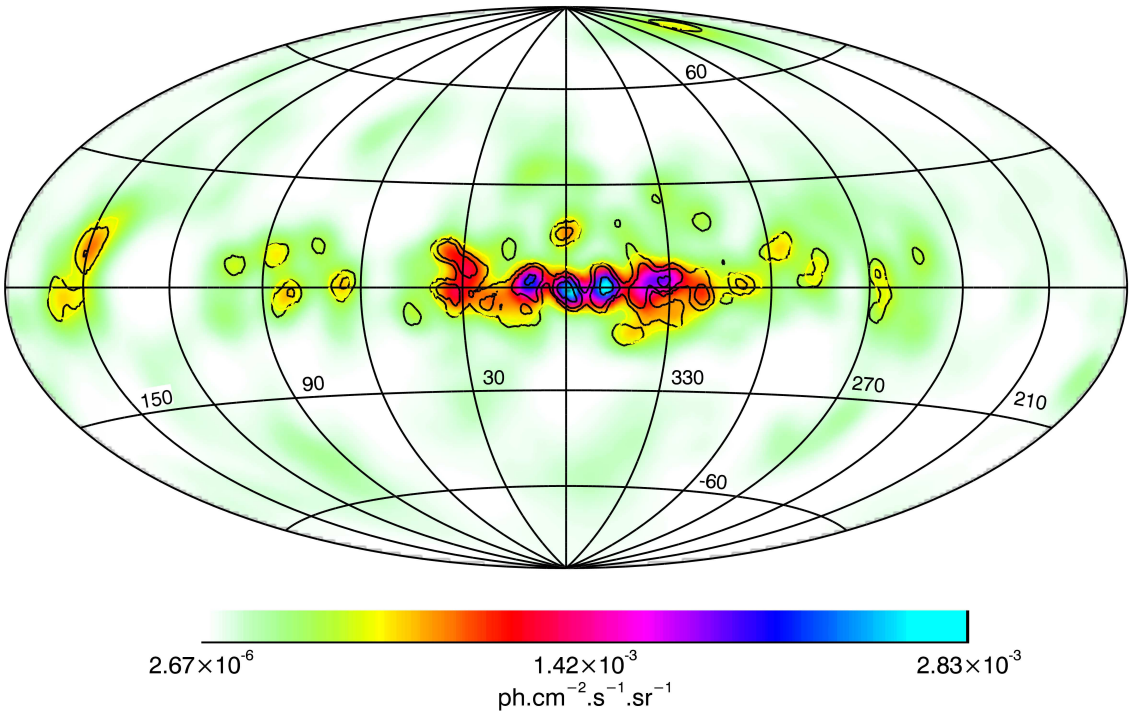

Figure 2: Image of the ^{26}Al line (1805-1813 keV). The resolution of the image is 6° FWHM. The contours are extracted from the 3° resolution image, in units of $\times 10^{-3}$ ph cm^{-2} s^{-1} sr^{-1}, they correspond to 0.6, 1.3, and 3.2. From left to right: Perseus region ($105° \leq l \leq 170°$) (Taurus clouds), the Cygnus/Cepheus region ($75° \leq l \leq 100°$), the inner Galaxy (-30° $\leq$ l $\leq$30°, -10° $\leq$ b $\leq$10°), Carina (l=286°, b=1°) and Vela region ($260° \leq l \leq 270°$). At mid-latitude, the Sco/Cen region ($300° \leq l \leq 360°$, 8 ° $\leq$ b $\leq$ 30°).

on Figure 2, shows that the emission is confined in the inner-Galaxy disk ($|l| \leq 30°$, $|b| \leq 10°$) with an estimated flux of $\sim 3.5 \times 10^{-4}$ph cm^{-2} s^{-1} .

Beyond the morphology of the diffuse emission, several spots are visible in the image. Some of them have positions compatible with sources detected or studied during recent SPI investigations ([11, 12, 13]) or appear in both SPI and *COMPTEL* data analyzes of [4] which reinforces their reliability.

In the Cygnus region ($72° < l < 96°$, $-7° < b < 7°$), the image reveals several excesses. A significant one is located at a position compatible with Cyg OB2 cluster (81°,-1°) as reported by [11].

We report for Cyg OB2 cluster a flux of $4.1-4.5\pm1.5\times10^{-5}$ photons cm^{-2} s^{-1} compatible with the value of $3.9\pm1.1\times10^{-5}$ photons cm^{-2} s^{-1} published by [11]. The Cygnus complex is also seen in the *COMPTEL* images.

The strongest excess visible in Sco-Cen region ($(328^\circ < l < 355^\circ$, $8^\circ < b < 30^\circ$) is localized at (l,b)$\approx$(360°, 16°), with a spatial extent around 5° radius. This position remains compatible with the position (l,b)=(350°,20°) and a spatial extension of 10° radius reported in [12]. This excess was detected with a high confidence level (the flux reported by [12] is $6\pm1\times10^{-5}$ photons cm^{-2} s^{-1}) with a somewhat different analysis. We report by using the same spatial extension and location as in [12] a maximum flux of $((4.2\pm1.6)\times10^{-5}$ photons cm^{-2} s^{-1} and by using the spatial extent and location from the image analysis a flux of $(4.1\pm1.6)\times10^{-5}$ photons cm^{-2} s^{-1}). However, the model-fitting analysis shows that the measured flux depends on the template which is used to model the large-scale emission of the ^{26}Al line (it is detected only above 2σ with an H_I template). We note that this feature is not reported by the *COMPTEL* data analysis.

There are also some structures around Carina and Vela regions. Their fluxes (respectively $(3.0\pm1.5)\times10^{-5}$ photons cm^{-2} s^{-1} and $(3.5\pm1.8)\times10^{-5}$ photons cm^{-2} s^{-1}) are comparable to the estimations reported for Carina [13] and for Vela (using *COMPTEL* data; [14]), but they are detected at low significance level (2σ).

We get also two significant and robust excesses, not previously reported by *COMPTEL*These excesses, rather extended, are seen in the Taurus/Anticenter ($105^\circ < l < 170^\circ$, $-15^\circ < b < 20^\circ$) region, with fluxes of $4-6\pm2$) and $(8-9\pm3)\times10^{-5}$ photons cm^{-2} s^{-1}. At least, we want to mention an excess at high-latitude ((l,b)$\approx$(226°,76°)) with flux $(7\pm2)\times10^{-5}$ photons cm^{-2} s^{-1}, for which we did not find any convincing potential counterpart, not previously reported.

5. SUMMARY

In the model-fitting analysis based on other wavelength maps, our data do not allow to distinguish a unique template since several one lead to similar likelihood parameter. From *COMPTEL* data, ([3]) had concluded that the best tracers were DIRBE 240μ and 53 GHz free-free maps. We agree that the FIR maps with wavelengths 60 to 240μ or 53 GHz (free-free and dust) appear to give statistically the best estimate of the ^{26}Al emission global morphology but CO, NIR A[4.9μ] and A[3.5μ] extinction-corrected maps have also to be considered with only a slightly lesser degree of confidence. In addition, âĂIJlow-contrastâĂİ maps observed at 25μ and 12μ provide an equally good description of the emission.

Our results confirm that the ^{26}Al emission follows more or less the distribution of the extreme Population I, the most massive stars in the Galaxy ([1]). It is known that the massive stars, supernovae and novae produce the long-lived isotopes ^{26}Al and ^{60}Fe with half-lives of 0.7 and 2.6 My. In addition, core collapse SNe produce dust/grains while massive star-supernovae are major dust factories, therefore dust FIR and MIR maps are expected to provide a good description of the emission. Quantitatively, the flux extracted through the model fitting method for the inner Galaxy ($|l|\leq30^\circ$,$|b|\leq10^\circ$) is found to be around 3.3×10^{-4}ph cm^{-2} s^{-1} while it does not depend much on the sky model (particularly if we restrict ourselves to the preferred ones). Similarly, [15] using a "light-bucket" method obtain a flux of 4×10^{-5} photons cm^{-2} s^{-1} for the region delimited by $|l|\leq40^\circ$,$|b|\leq40^\circ$. For the same region, we obtain a flux of $\sim3.9\times10^{-4}$ph cm^{-2} s^{-1} with the

most probable spatial morphologies. Our measured flux is consistent with earlier measurements of both *INTEGRAL*/SPI and *COMPTEL* instruments.

Another observable quantity, related to ^{26}Al production is the ratio between ^{60}Fe and ^{26}Al line fluxes in the inner Galaxy. With our analysis, the ^{60}Fe mean flux in the inner Galaxy is about 4×10^{-5} photons cm^{-2} s^{-1}, leading to a ^{60}Fe to ^{26}Alłratio between 0.12 and 0.15. Considering the numerous uncertainties still affecting these models, this results confirms those reported by [16, 17].

A more direct comparison of SPI and *COMPTEL* data shows that the ^{26}Al line is detected at $\sim 20\sigma$ using SPI data, to be compared to the $\sim 30\sigma$ obtained with the analysis of *COMPTEL* data ([3]).

Finally, in addition to the most robust feature in the Cygnus region, the SPI image indicates important spots at l$\simeq$330° and l$\simeq$320° and two features, which we tentatively associated to Taurus/Anticenter region. This could be correlated to *COMPTEL* MREM image ([3]), for which it is mentioned, two spots at l$\simeq$317° and l$\simeq$332° and an extended emission around (l, b) $\simeq$(160°,0°).

Some improvements in the data analysis appear achievable to still refine the results. In particular, an accurate modeling of the response outside the field-of-view is a prime objective for studying emissions above $\sim$1 1 MeV.

References

[1] Diehl, R., Bennett, K., Bloemen, et al., 1995, *A & A* , 298, L25

[2] Oberlack, U., Bennett, K., Bloemen, H., et al., 1996, *A & A sup. series*, 120, 311

[3] Knödlseder, J., Bennett, K., Bloemen, H., et al., 1999, *A & A* , 344, 68

[4] Plüschke, S., Diehl, R., Schoenfelder, V., et al., Proceedings of the Fourth INTEGRAL Workshop, ESA SP-459, 2001

[5] Chen, W., Gehrels, N., Diehl, R. and Hartmann, D., 1996, A&AS, 120, 315

[6] Kretschmer, K., Diehl, R., Krause, M. et al., 2013, aap, 559, 99

[7] Vedrenne, G., Roques, J. P., Schonfelder, V., et al., 2003, *A & A* , 411, L63

[8] Roques, J. P., Schanne, S., Von Kienlin, A., et al., 2003, *A & A* , 411, L91

[9] Bouchet,L., Jourdain, E. & Roques, J.-P., 2015, ApJ, 801, 142

[10] Skilling, J. & Bryan, R. K., 1984, *MNRAS*, 211, 111

[11] Martin, P., Knödlseder, J., Diehl, R. & Meynet G., 2009 *A & A* , 506, 703

[12] Diehl, R., Lang, M.G., Martin, P. et al., 2010, *A & A* , 522, A51

[13] Voss, R., Martin, P., Diehl, R., et al., 2012, *A & A* , 539, 66

[14] Diehl, R., Bennett, K., Bloemen, et al., 1995a, *A & A* , 298, L25

[15] Churazov, E., Sazonov, S., Ysygankov S., et al., 2011, *MNRAS*, 411, 1727

[16] Harris, M. J, Knödlseder, J., Jean, P., et al., 2005, *A & A* , 433, L49

[17] Wang, W., Harris, M. J., Diehl, R., et al., 2007, *A & A* , 469, 1005